A Study on the Capacity Fading and the Replacement of Surface Film at the Surface of LiMn$_2$O$_4$ Thin Film Electrode

Prof. Kwang-Bum Kim

(Yonsei University)

A Study on the Capacity Fading and the Replacement of Surface Film at the Surface of LiMn$_2$O$_4$ Thin Film Electrode

Kyung Yoon Chung, Dong Shu, and Kwang-Bum Kim
Dept. of Metallurgical Eng., Yonsei Univ.

Abstracts

The presence of tetragonal phase at the surface of LiMn$_2$O$_4$ particle due to a Jahn-Teller effect was previously reported to be one of the causes for capacity fading observed during cycling of Li//Li$_x$Mn$_2$O$_4$ in 4V range. Further, it is reported that a Jahn-Teller effect in 4V range may be suppressed by substitution of Mn ions with Li ions or other transition metal ions. However, the direct evidence of the suppression of a Jahn-Teller effect in 4V range by substitution of Mn ions with other metal ions has not been reported. The dissolution and formation of surface film at the surface of LiMn$_2$O$_4$ electrodes also reportedly affect the capacity fading or rate capability. This study reports on the evidence of the onset and suppression of a Jahn-Teller effect in 4V range and the dissolution and formation of surface film at the surface of LiMn$_2$O$_4$ thin film electrodes using in situ bending beam method (BBM) in situ electrochemical quartz crystal microbalance (EQCM).

Introduction

There has been rapid progress in the portable electronics industry and this led to a great increase for the demand of portable, lightweight power sources, and lithium secondary batteries have met these demands. At present, LiCoO$_2$ is widely used as a cathode material, but LiMn$_2$O$_4$ is an excellent alternative material in view of its several advantages like low cost, easy availability of raw materials and environmental benignity. However, LiMn$_2$O$_4$ has a disadvantage of capacity fading during cycling. Many factors have been proposed to contribute to the capacity fade in 4V range, and one of them is the onset of a Jahn-Teller effect at the end of discharge. Thackeray et al. reported the onset of a Jahn-Teller effect at the end of discharge in 4V range using TEM, which is ex situ technique.[1,2] And, we previously reported the evidence of the onset of a Jahn-Teller effect in 4V range using in situ BBM.[3] And, several authors reported that the onset of a Jahn-Teller effect can be suppressed by the substitution of Mn ions with other metal ions.[2] Further, several authors reported the ex situ evidence of the dissolution and formation of surface film at the surface of LiMn$_2$O$_4$ electrode, and mentioned that this films may induce capacity fading or affect rate capability.[4,5]

In this study, the direct evidence of the suppression of a Jahn-Teller effect by substituting Mn ions with other metal ions (Co^{3+}, Ni^{2+}) and dissolution and formation of surface film at the surface of LiMn$_2$O$_4$ electrodes using in situ BBM and EQCM are shown.

Experimental

Synthesis of LiM$_\delta$Mn$_{2-\delta}$O$_4$ (M=Co and Ni; δ=0 and 0.05) thin film electrodes was carried out by electrostatic spraying deposition (ESD) technique[3,6] and the detailed synthesis parameters are described in our previous report.[3]

The in situ strain measurements of the electrodes were carried by means of BBM. The schematic representations of the in situ BBM system and a cantilever system of the working electrode are shown and explained in detail in previous reports.[3,7] The electrochemical cell used for BBM was a beaker cell made of Teflon with three electrodes fixed on the plastic cap that hermetically closed the cell.

The frequency change of quartz crystal during cyclic voltammetry is measured with EQCM (Seiko EG&G),[6,8] and the measured frequency can be converted to mass change using Sauerbrey equations.[9] The electrochemical cell used for EQCM was sealed in a stainless steel chamber.
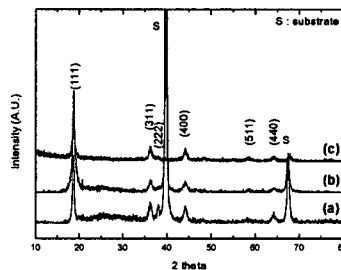
Results & Discussion

Fig. 1. XRD pattern of thin film LiM$_\delta$Mn$_{2-\delta}$O$_4$. (a) LiMn$_2$O$_4$, (b) LiCo$_{0.05}$Mn$_{1.95}$O$_4$, (c) LiNi$_{0.05}$Mn$_{1.95}$O$_4$.

The XRD patterns of LiM$_\delta$Mn$_{2-\delta}$O$_4$ (M=Co and Ni, δ=0, 0.05) synthesized by ESD technique are shown in Fig. 1. The peaks marked "S" are from the substrate. All the XRD patterns could be indexed to the cubic spinel of space group Fd3m.

It has been previously reported that a Jahn-Teller effect takes place when the average oxidation state of Mn ions becomes lower than 3.5.[11] The initial average oxidation state of stoichiometric LiMn$_2$O$_4$ is 3.5 and that of Li$_{1-x}$Mn$_2$O$_4$ becomes greater as the x value becomes greater, and theoretically the average oxidation state of Mn ions in fully charged state of spinel oxide should be 4+. When stoichiometric spinel oxide is fully discharged, the average oxidation state of Mn ions should be 3.5, and there should not be a Jahn-Teller effect. But, according to Thackeray et el., at non-equilibrium, dynamic conditions, due to the accumulation of lithium ions at the surface of spinel oxide, the average oxidation state of Mn ions at the surface of the

spinel particle will fall below 3.5, and a Jahn-Teller distortion will take place in 4V range.[1,2] However, if the average oxidation state of Mn ions of spinel oxide in fully discharged state could become slightly greater than 3.5, even for lithium ions accumulation at the surface of spinel oxide particle, the onset of a Jahn-Teller effect would be suppressed. Thus this will lead to the improvement of cycleability. This hypothesis is previously reported by Thackeray et el. that by substituting Mn ions with lithium ion or other transition metal ions, a Jahn-Teller effect may be suppressed.[1,2] But, the direct evidence of the suppression of the Jahn-Teller effect in 4V range has not been reported to the best of our knowledge. In the present study, we report the direct evidence of the onset and suppression of the Jahn-Teller effect in 4V range of $LiM_\delta Mn_{2-\delta}O_4$ (M=Co and Ni; δ=0 and 0.05) electrode using in situ BBM.
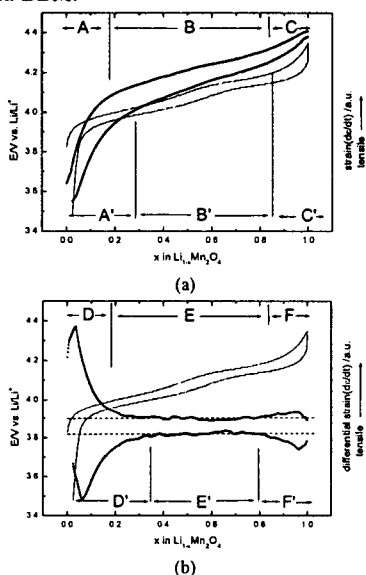

Fig. 2. (a) Strain curves (thick line) and (b) differential strain curves (thick line) superimposed on the galvanostatic charge/discharge curves of thin film $LiMn_2O_4$. Applied current: 20 μA. The dashed lines in (b) are the reference lines.

Fig. 2 shows the strain and differential strain curves of the second cycle superimposed on the galvanostatic charge/discharge curves of thin film $LiMn_2O_4$ electrode. The strain curve in Fig. 2(a) can be divided into three regions, which are designated A-A', B-B', and C-C'. Region B-B' shows the gentlest slope and region A-A' shows the steepest slope. And similar to the galvanostatic charge/discharge curve, the strain curve shows a little hysteresis between the strain curves of charge and discharge. These slope variations can be observed more clearly with differential strain curve. In Fig. 2(b), the differential strain curve is shown, and it can be divided into three regions as in the strain curve, and it is designated D-D', E-E', and F-F'. The differential strain curve shows a large peak in region D-D' and constant value in region E-E'. A small hump is observed in region F.

According to the previous report by Ohzuku et el.,[10] the

lattice parameter of $LiMn_2O_4$ changes linearly with charge/discharge in 4V range, and there is sudden jump due to a Jahn-Teller effect when charged/discharged out of/into 3V range. Therefore, if the spinel electrode is cycled within 4V range, the strain variation should be proportional to the amount of lithium ions inserted or extracted, and the differential strain curve should show constant value. But, the strain and differential strain curves in Fig. 2 deviates from the expectation of the previous report. However, in the recent report by Thackeray et el., there is the onset of a Jahn-Teller effect at the end of discharge even in 4V range,[1,2] and it will influence the strain during galvanostatic charge/discharge. Thackerey et el. observed the formation tetragonal phase in the spinel electrodes, which are discharged to 3.0, 3.3, and 3.5V, respectively. This reveals that the onset of a Jahn-Teller effect takes place above 3.5V, and we can predict that there should be drastic strain variation above 3.5V during discharge.

The differential strain curve in Fig. 2(b) follows the prediction very well. The large compressive peak in the region D' of differential strain curve during discharge indicates that there is drastic volume expansion that is larger than that in region B'. The counterpart peak in region D during charge is due to the relaxation of tetragonal phase, which is formed during previous discharge, into cubic phase. Due to the repetitive onset and relaxation of a Jahn-Teller effect, some of the active mass may lose the electronic contact with bulk electrode, and it contributes to the capacity loss.

To investigate the onset and relaxation of a Jahn-Teller effect during cyclic voltammetry, we measured the strain variation during cyclic voltammetry. Fig. 3(a) shows the strain curve of the second cycle superimposed on the cyclic voltammogram of thin film $LiMn_2O_4$ measured at a scan rate of 1mV/s. Similar to the galvanostatic charge/discharge, tensile strain is experienced during lithium extraction and compressive strain during lithium insertion. As stated earlier, the strain variation should be proportional to the amount of lithium ions inserted/extracted, that is, the differential strain (dε/dQ) curve should have the constant value, which is the same situation as in the galvanostatic charge/discharge. Fig. 3(b) shows the differential strain (dε/dQ) curve of the second cycle, which is calculated from the data of Fig. 3(a). It should be noted that the differential strain (dε/dQ) curve is very similar to that of the galvanostatic charge/discharge. The differential strain (dε/dQ) curve in Fig. 3(b) also can be divided into three regions, which is designated I - I', II - II', and III - III'. During anodic scan, the differential strain (dε/dQ) curve shows positive value, which is tensile strain, and during cathodic scan negative value, which is compressive strain. In region II - II', it shows constant value and follows the postulation that is derived from the result of Ohzuku el el.'s report.[10] But, region I - I', similar to the region D-D' in Fig. 3(b), shows the strain much larger than region II - II'. This larger value of strain in region I - I' can also be attributed to the onset and relaxation of a Jahn-Teller effect. Furthermore, the potentials where the deviation of differential strain value in region I - I' and D-D' from

the constant value of region Ⅱ-Ⅱ′ and E-E′ is observed are ca. 3.97 and 3.99V, respectively.
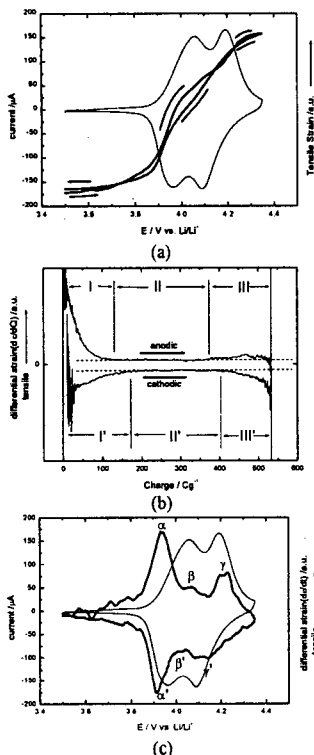

(a)

(b)

(c)

Fig. 3. (a) Strain curves (thick line) and differential strain curves - (b) dε/dQ, (c) dε/dt (thick line) -superimposed on the cyclic voltammograms of thin film LiMn$_2$O$_4$. Scan rate: 1mV/s.

From above results, we can conclude that even in the cyclic voltammetry, a Jahn-Teller effect takes place at the end of cathodic scan. The onset and relaxation of a Jahn-Teller effect shows up as additional peaks in differential strain (dε/dt) curves at potentials around 3.9V. Fig. 3(c) shows the differential strain (dε/dt) curve superimposed on the cyclic voltammogram. According to the postulate previously described, differential strain (dε/dt) curve should have the same shape as cyclic voltammogram. The differential strain (dε/dt) curve shows three pairs of peaks which are designated α-α′, β-β′, and γ-γ′. The peaks β-β′ are almost buried under the feet of large peaks α-α′. Two pairs of peaks, β-β′ and γ-γ′, can be attributed to two pairs of current peaks in cyclic voltammogram, and the peaks α-α′ can be attributed to the onset and relaxation of a Jahn-Teller effect.

If the insertion rate of lithium ions during discharge or cathodic scan is greater than the diffusion rate of lithium ions from the surface into the bulk matrix of LiMn$_2$O$_4$, there will be the accumulation of lithium ions at the surface of LiMn$_2$O$_4$ particle, making the average manganese valence at the surface of the particle to fall below 3.5. Therefore, a Jahn-Teller effect is induced and the cubic phase at the surface of LiMn$_2$O$_4$ particle will be transformed to tetragonal phase. When cubic phase is transformed into tetragonal phase, there is 5.6% expansion

in volume, which is rather abrupt change compared with the volume expansion due to lattice parameter change within cubic phase.[10] Therefore, it is observed as an additional peak with a large magnitude in differential strain curves. When the tetragonal phase is formed on the surface of LiMn$_2$O$_4$ particle due to a Jahn-Teller effect, there is a misfit between cubic phase of bulk and tetragonal phase of surface, thus some of the tetragonal phase may dissociate from the bulk electrode, and leads to the capacity fading.

The substitution of Mn ions with other transition metal ions, which have lower valence than Mn ions, will increase the average valence of Mn ions. This gap between the average oxidation states of Mn ions in substituted spinel oxide and stoichiometric spinel oxide-LiMn$_2$O$_4$ will work as a cubic 'buffer' zone that suppresses the onset of a Jahn-Teller effect at the end of discharge or cathodic scan at the surface of spinel particles. To evaluate the influence of doping on the Jahn-Teller effect, we prepared two sets of transition-metal-ions-substituted spinel oxide, which are LiCo$_{0.05}$Mn$_{1.95}$O$_4$ and LiNi$_{0.05}$Mn$_{1.95}$O$_4$. It is previously reported by several authors that Co ions resides in the oxidation state of 3+ and Ni ions 2+ in spinel oxide.[12] Therefore, when a part of Mn ions are substituted by other transition metal ions, which have the oxidation state of 3+ or 2+, the average valence of Mn ions will be increased. As the valence of doping ions become lower or the amount of doping increases, the extent of cubic 'buffer' zone increases, and the suppression effect will be more effective.
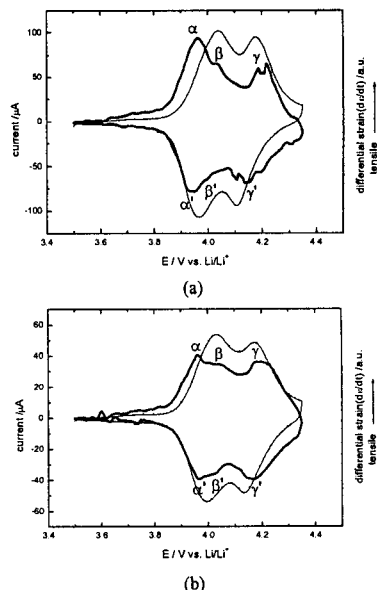

(a)

(b)

Fig. 4. Differential strain curves (thick line) superimposed on the cyclic voltammograms (thin line) of thin film LiM$_\delta$Mn$_{2-\delta}$O$_4$. (a) LiCo$_{0.05}$Mn$_{1.95}$O$_4$, (b) LiNi$_{0.05}$Mn$_{1.95}$O$_4$.

Fig. 4 shows differential strain curves of the second cycle superimposed on the cyclic voltammetry of LiM$_{0.05}$Mn$_{1.95}$O$_4$ (M=Co, Ni). In Fig. 4(a), it is observed that the peak α-α′ is much reduced compared to that of Fig. 3(c), especially the reduction of the magnitude of peak α′ is more pronounced. Because Mn ions, which have the

average oxidation state of 3.5 in the stoichiometric $LiMn_2O_4$, are substituted with lower valence Co^{3+} ions, the average oxidations state of Mn ions becomes greater. In case of $LiCo_{0.05}Mn_{1.95}O_4$, the average oxidation state of Mn ions is ca. 3.513. As the average oxidation state of Mn ions at the end of cathodic scan in cyclic voltammetry is greater than 3.5, there is a cubic 'buffer' zone, which hinders the falling of the oxidation state of Mn ions at the surface below 3.5 at the end of cathodic scan, and suppress the onset of a Jahn-Teller effect. The further suppression of a Jahn-Teller effect in 4V range is more pronounced when the valence of dopant ions is decreased. Fig. 4(b) shows the differential strain curves and cyclic voltammograms of $LiNi_{0.05}Mn_{1.95}O_4$. It is observed that the magnitude of the peak α' is much more decreased compared to that of Co^{3+} doped spinel. This is due to the lower valence of Ni ions than that of Co ions. The oxidation state of Ni ions is 2+, and when the same amount of dopant is substituted into spinel oxide, the Ni ions increase the average oxidation state of Mn ions more effectively than Co ions do. The average oxidation state of Mn ions in $LiNi_{0.05}Mn_{1.95}O_4$ is 3.538. This value is greater than that of Co doped spinel oxide in this study. Therefore, there is greater cubic 'buffer' zone in Ni doped spinel oxide than Co^{3+} doped spinel oxide, and Ni^{2+} doped spinel oxide will suffer less extent of a Jahn-Teller effect in 4V range. This is observed in Fig. 4(b). The magnitude of the peak α' is much more decreased than that of Fig. 4(a).
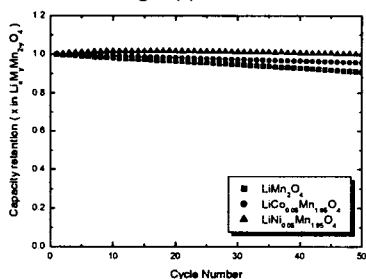

Fig. 5. Capacity retention (x in $Li_xM_yMn_{2-y}O_4$ vs. cycle number) calculated from the cyclic voltammograms.

Fig. 5 shows discharge capacity retention of $LiMn_2O_4$, $LiCo_{0.05}Mn_{1.95}O_4$, and $LiNi_{0.05}Mn_{1.95}O_4$ thin film electrode. It is seen from Fig. 5 that all three thin film electrodes prepared by ESD technique show very stable cycling characteristics. From the capacity retention curve in Fig. 5, it can be observed that $LiNi_{0.05}Mn_{1.95}O_4$ shows the best capacity retention followed by $LiCo_{0.05}Mn_{1.95}O_4$ and $LiMn_2O_4$. The capacity retentions after 50 cycles are 90.85% and 95.64% for $LiMn_2O_4$ and $LiCo_{0.05}Mn_{1.95}O_4$, respectively. And $LiNi_{0.05}Mn_{1.95}O_4$ showed almost no capacity loss up to 50 cycles. From the results in Fig. 4(a) and (b), this improvement in cycleability by doping is thought to be in great part due to the suppression of a Jahn-Teller effect around 3.90~3.95V.

Using BBM, we could also observed the strain variation due to surface film replacement. Fig. 6 shows the strain curves superimposed on the expanded view of the cyclic voltammograms in different electrolytes. The cutoff voltages were 3.5~4.35V, and the scan rates were 1mV/s.

The electrolytes used were 1M $LiClO_4$/PC, 1M $LiPF_6$/EC-DMC, and 1M $LiClO_4$/EC-DEC for Fig. 6(a), (b), and (c), respectively. The observation of the cyclic voltammograms reveals that the current responses in different electrolytes show different characteristics. The current peaks in Fig. 6(a) are broader than that in Fig. 6(b) and that of Fig. 6(c) are the narrowest. The dependence of electrochemical characteristics of cathode electrode on the composition of electrolytes are previously reported,[13] and it was reportedly related to different ionic conductivities of electrolytes. And similar to previous report, our results can also be attributed to the difference of electrolyte. However, there may be factors other than ionic conductivities that can contribute to the different electrochemical characteristics of cathode electrode.
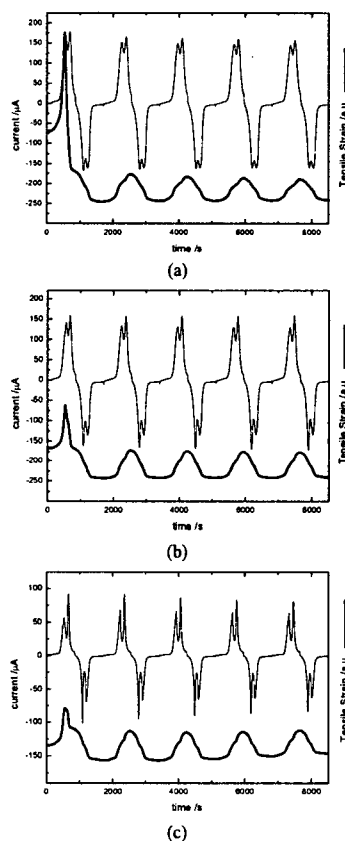

(a)

(b)

(c)

Fig. 6. Expanded view of strain curves (thick line) superimposed on cyclic voltammograms (thin line) to 5 cycles. Scan rate: 1mV/s, electrolytes: (a) $LiClO_4$/PC, (b) $LiPF_6$/EC-DMC, (c) $LiClO_4$/EC-DEC

The strain curves showed similarities and differences among one another. The similarities are the larger tensile peak in the first cycle compared to those from the second cycle forth, and the same shape of the strain curve from the second cycle forth, which is due to lithium insertion/extraction into/out of spinel matrix.[3] It should be noted that this strain variation from the second cycle on is experienced in the region of compressive strain. Further, the large tensile strain peak position in the first cycle of strain curves did not change significantly for the

electrolytes used. The peak positions were 4.037, 4.040, and 4.050V for Fig 6(a), (b), and (c), respectively.
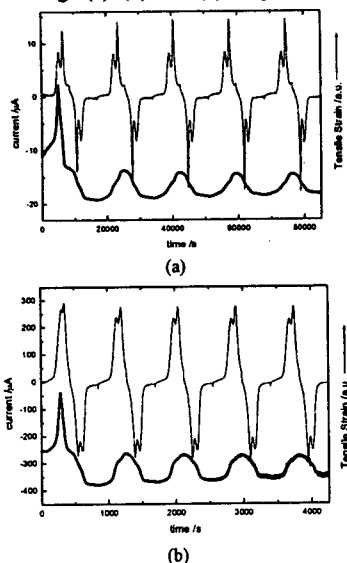

(a)

(b)

Fig. 7. Expanded view of strain curves (thick line) superimposed on cyclic voltammograms (thin line) to 5 cycles. Scan rate: (a) 0.1mV/s, (b) 2mV/s, electrolyte: (a) LiClO₄/PC, (b) LiPF₆/EC-DMC

Cyclic voltammograms were measured at different scan rates and in different electrolytes to determine whether the peak position is dependent on immersion time or potential of the electrode. Fig. 7(a) and (b) show the strain curves and cyclic voltammograms at 0.1 and 2mV/s, respectively. Electrolytes used were 1M LiClO₄/PC and 1M LiPF₆/EC-DMC. If the factors that contribute to the peak were dependent on the immersion time, the peak position would change as the time to reach a certain potential depends on the scan rate. However, even with the different scan rates and the different electrolytes, tensile strain peaks appeared at potentials close to those of Fig. 6. The peak positions were 4.037 and 4.040V for Fig. 7(a) and (b), respectively.

From these results, it could be summarized that the evolution of tensile strain peak depends on the potential regardless of the electrolytes used in this study and its magnitude varies depending on the electrolytes used. Furthermore, comparison of the strain curves in Fig. 6 and 7 in the same electrolytes reveals that the magnitudes of strain curves in the first cycle increase as the scan rate increases.

From the second cycle forth, the strain variation can be successfully explained by the lattice parameter change due to lithium insertion/extraction and phase transformation between cubic and tetragonal phases. But, as seen in Fig. 6 and 7, the tensile strain of the first cycle far exceeds the strain that is expected to come from lattice parameter change due to lithium insertion/extraction or phase transformation in 4V range and may be attributed to the dissolution/formation of surface film.

If there is surface film dissolution or formation on the electrode, it should naturally accompany mass change. Therefore, we measured the mass change during cyclic voltammetry, and Fig. 8(a) and (b) show the frequency change curves of the EQCM experiments of the first and second cycle superimposed on the cyclic voltammograms, respectively. Scan rate was 0.1mV/s and electrolyte used were 1M LiClO₄/EC-DEC. Mass (not shown) can be calculated from the frequency using Sauerbrey equation, and it is linearly proportional to the frequency.[9]
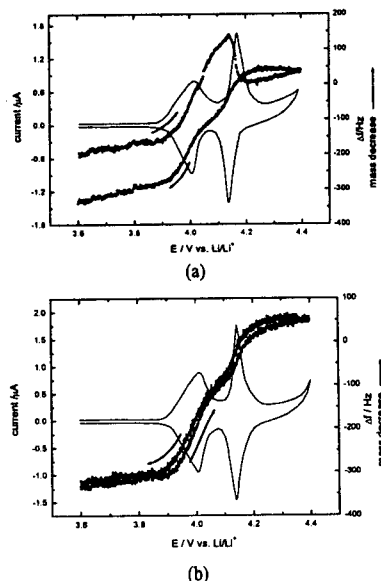

(a)

(b)

Fig. 8. Frequency (or mass) curves (thick line) of the (a) first and (b) second cycle superimposed on the cyclic voltammograms. Scan rate : 0.1mV/s. Electrolyte : LiClO₄/EC-DEC.

Theoretically, if the lithium ions are extracted from spinel matrix, there should be mass decrease, and if inserted, vice versa. Similar to strain curves, the frequency curve from the second cycle forth depicts this postulate very well. The frequency curve in Fig. 8(b) shows no hysteresis and complete mass recovery in frequency curve. Therefore, we can come to the conclusion that the frequency changes from the second cycle forth are mainly due to lithium ions insertion/extraction. However, as was observed in the strain curves, a large frequency peak was observed in the first cycle, which indicates initial large mass decrease followed by mass increase. This is a significant deviation from the theoretical consideration.

For easier comparison and assessment of the contribution of lithium insertion/extraction from others in the first cycle of strain and frequency curves, we superimposed the strain and frequency curves of the first and second cycle as shown in Fig. 9. In Fig. 9(a) are shown the strain curves of the first and second cycle superimposed on each other. These strain curves are taken from that of Fig. 6(c) and the second cycle is shifted up for easier comparison. As described in the postulate above, the second cycle strain curve shows tensile and compressive strain in anodic and cathodic scan, respectively. And there is little hysteresis in the second cycle curve. The strain curve of the cathodic scan of the first cycle shows similar behavior with that of the second cycle. However, the strain curve of the anodic scan of the first cycle shows quite different behavior from that of the second cycle. Unlike in
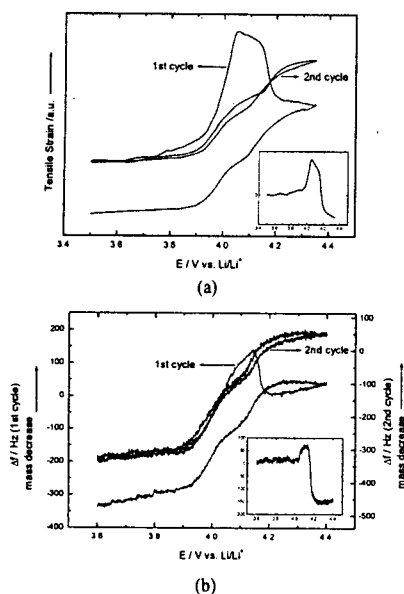
(a)

(b)

Fig. 9. (a) Strain and (b) mass change curves of the first and second cycle superimposed each other. The inset shows the difference of the strain and frequency in anodic scan between the first and second cycle. Scan rate : (a) 0.1mV/s, (b) 1mV/s, Electrolyte : LiClO₄/EC-DEC

the second cycle, the first cycle shows large tensile peak in the anodic scan, which represents large tensile strain followed by compressive strain. The frequency curves in Fig. 9(b) are similar to the strain curves in Fig. 9(a) in shape. In the second cycle, it shows mass decrease in anodic scan, and mass increase in cathodic scan without hysteresis. The frequency curve of the first cathodic scan shows very similar behavior with that of the second cathodic scan. However, the frequency curve of the first anodic scan shows much difference with that of the second anodic scan. In the first anodic scan, it shows large mass reduction peak, which is large mass reduction followed by large mass increase. The behaviors depicted in the frequency curves of Fig. 9(b) are very similar to that of strain curves in Fig. 9(a). During anodic scan, the strain and frequency curves of the first cycle begin to deviate from those of the second cycle at ca. 3.75 and 4.03V, respectively. The deviation of the curve appears at less positive potential in strain curve. Similarly, the peak positions of the strain curve precede that of frequency curve, and the peak positions are located at ca. 4.055 and 4.14V, respectively.

From the postulate described above, we can assume that only the lithium ion insertion and extraction cause the strain and frequency variation from the second cycle forth. However, in the first cycle, lithium ion insertion/extraction and other factors contribute to the strain and frequency variation. Therefore, to eliminate the contribution of lithium insertion/extraction and to observe the contribution of the other factors in the first cycle, we calculated the difference between the first and second cycles of the strain and frequency curves. The insets in Fig. 9(a) and (b) show the differences between the first and second anodic cycles. Because the difference in the contribution of lithium ion

insertion/extraction to the strain and frequency in the first and second is expected to be negligible, the strain difference curve and frequency difference curve in insets will depict the contribution of the factors other than lithium insertion/extraction.

The inset in Fig. 9(a) shows constant value of strain difference at the beginning of the anodic scan followed by the peak with further potential scan. The peak position is 4.047V. Beyond the peak, the strain difference decreases rapidly crossing the baseline, i.e. the strain difference value becomes negative. The negative value of the strain difference depicts that the strain became more compressive than at the beginning of the anodic scan. Similar to the strain difference curve, the frequency difference curve in the inset of Fig. 9(b) shows constant values of frequency difference at the beginning of anodic scan followed by the peak with further potential scan. The peak position is located at 4.11V. Beyond the peak, the frequency difference also decreases rapidly crossing the baseline, i.e. the frequency difference value becomes negative, and it depicts the mass increase beyond that of the beginning part of the anodic scan.

The comparison of the peak positions in the curves of the insets shows that the difference became even smaller compared to those in strain and frequency curve. Its peak positions for strain and frequency difference curves are 4.047 and 4.11V, respectively, and its difference is only 63mV. These small differences can be attributed to the difference in experimental factors such as thickness and dimension of the electrodes for strain and EQCM measurements. Therefore, it could be said that the strain and frequency changes observed in the first anodic scan are correlated to each other, that is, the abnormal occurrence of the peak in the first anodic scan of strain and frequency curves represents the contribution of the factors other than lithium insertion/extraction. And, the factors other than lithium insertion/extraction influence the strain and frequency variations, respectively, over the similar potential domain.

In the previous report by Aurbach et el., the active mass of the electrode is always covered by surface film.[5] The pristine electrodes are covered with Li₂CO₃ which is formed during the synthesis route, and after cycling in the electrolytes at room temperature it is replaced with electrolyte-related surface film. However, they only observed this dissolution and formation of surface film via ex situ techniques, therefore they could not follow the variation of the surface film during cycling and get the potential range where this replacement take places.

From our experimental results and other reports,[4-6] we could conclude that the initial tensile strain and mass reduction are due to the dissolution of initially formed surface film, which is Li₂CO₃ layer, and subsequent compressive strain and mass increase are due to the formation of new electrolyte-related surface film. The dissolution of initially formed surface film and formation of new surface film depend on the applied potential, and the formation of electrolyte related surface film is activated at potentials around 4.1V. The replacement process of surface layer is mostly finished during the first anodic scan.
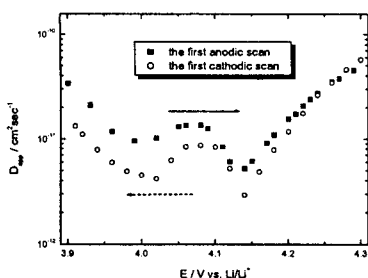
Fig. 10. Dependence of the apparent chemical diffusion coefficient (D_{app}) on the electrode potential; potential step: 10mV

The replacement of the initial surface film with the new surface film may alter the process at or across the surface film layer. When lithium ions are inserted/extracted into/out of the spinel electrodes, they inevitably migrate through the surface film formed at the surface of electrodes. Therefore, the different characteristics of the surface film of the initial and new ones may influence the electrochemical characteristics of the spinel electrodes, because the different chemical diffusion coefficients or insulating characteristics of the surface film nay affect the kinetics or impedance of the electrode. Thus, to confirm the postulate derived above, we measured D_{app} at various electrode potentials using potential-step chronoampero-metry technique and it is shown in Fig. 10.[14] In the first upward potential step, it showed steady decrease of D_{app}, followed by two peaks, which is located at the potential range where two current peaks are observed in cyclic voltammograms, and steady increase toward the end. In the consecutive downward potential step, the D_{app} value follows the trail of the D_{app} value of the first upward potential step in the beginning. It also shows two peaks in the middle and steady increase at the end. However, it deviates from that of the first upward potential step around 4.1V. In the potential range below 4.1V, D_{app} value of the downward potential step is smaller than that of the upward potential step. The similar behavior was also observed by Nishizawa et el.[14] The onset potential where the deviation of D_{app} value is observed coincides very well with that of strain and frequency curve. This difference in D_{app} values in anodic and cathodic scan below ca. 4.1V may be due to the different nature of the film that covers the electrode. Above ca. 4.1V, both in anodic and cathodic scan, the surface film is already replaced with electrolyte related film. Therefore, D_{app} values remain unchanged. But, below ca. 4.1V, the surface layer during anodic scan is Li_2CO_3 and that during cathodic scan is electrolyte-related surface film, therefore, D_{app} also shows different values.

Conclusion

The evidence of the onset of a Jahn-Teller effect in thin film $LiMn_2O_4$ and suppression of a Jahn-Teller effect by the substitution of Mn ions with other transition metal ions (Co^{3+}, Ni^{2+}) during cyclic voltammetry in 4V range is detected by BBM. The strain data were obtained simultaneously with electrochemical signals, and the differential strain curves were analyzed in conjunction with electrochemical data to examine the onset and suppression of a Jahn-Teller effect in thin film $LiM_\delta Mn_{2-\delta}O_4$ electrode in 4V range.

The suppression of a Jahn-Teller effect by substituting Mn ions with other metal ions are probed by the variation of the magnitude of the additional peaks. The magnitude of this additional peak became smaller when doped with metal ions having lower valence than Mn ions. As expected from the differential strain curves, Ni^{2+} substituted spinel showed the best cycleability without little capacity fade up to 50th cycle.

Further, the evidence of dissolution of initially formed surface film and formation of new electrolyte related surface film on $LiMn_2O_4$ thin film electrode during cyclic voltammetry is investigated by in situ BBM, EQCM, and measurement of D_{app}. During the first anodic scan, the replacement of surface film is terminated. The formation of electrolyte related surface film initiates at ca. 4.03~4.1V. Due to the different nature of surface films before and after replacement, D_{app} show different value below ca. 4.1V between the first anodic and cathodic scan. Therefore, it can be concluded that the replacement of surface film is dependent on applied potential.

References

1. M. M. Thackeray, Y. Shao-Horn, A. J. Kahaian, K. D. Kelper, E. Skinner, J. T. Vaughey, and S. A. Hackney, *Electrochem. Solid-State Lett.*, Vol. 1, pp 7, 1998
2. R. J. Gummow, A. de Kock, and M. M. Thackeray, *Solid State Ionics*, Vol. 69, pp 59, 1994
3. K. Y. Chung and K.-B. Kim, *J. Electrochem. Soc.*, Vol. 149, pp A79, 2002
4. Y. Matsuo, R. Kostecki, and F. McLarnon, *J. Electrochem. Soc.*, Vol. 148, A687(2001)
5. D. Aurbach, K. Gamolsky, B. Markovsky, G. Salitra, Y. Gofer, U. Heider, R. Oesten, and M. Schmidt, *J. Electrochem. Soc.*, Vol. 147, 1322(2000)
6. T. Uchiyama, M. Nishizawa, T. Itoh, and I. Uchida, *J. Electrochem. Soc.*, Vol. 147, pp 2057, 2000
7. J. M. Rosolen and F. Decker, *J. Electrochem. Soc.*, Vol. 143, pp 2417, 1996
8. K. W. Nam and K. B. Kim, *J. Electrochem. Soc.*, Vol. 149, A346, 2002
9. G. Z. Sauerbrey, *Application of Piezoelectric Quartz Crystal Microbalance*, C. Lu and A. W. Czanderna, Editors, p. 26, Elsevier Press, New York (1984)
10. T. Ohzuku, M. Kitagawa, and T. Hirai, *J. Electrochem. Soc.*, Vol. 137, pp 769, 1990
11. K. Miura, A. Yamada, and M. Tanaka, *Electrochimica Acta*, Vol. 41, pp 249, 1996
12. L. Guohia, H. Ikuta, T. Uchida, and M. Wakihara, *J. Electrochem. Soc.*, Vol. 143, pp 178, 1996
13. M. Morita, O. Yamada, K. Adachi, M. Ishikawa, *Denki Kagaku*, Vol. 66, pp 1304, 1998
14. M. Nishizawa, T. Uchiyama, K. Dokko, K. Yamada, T. Matsue, and I. Uchida, *Bull. Chem. Soc. Jpn.*, Vol. 71, pp 2011, 1998